CHEMISTRY OF MATERIALS

Article

pubs.acs.org/cm

Colloidal Stability of Graphene-Based Amphiphilic Janus Nanosheet Fluid

Dan Luo,[†,‡] Feng Wang,[†] Md Kamrul Alam,[§] Fang Yu,[†] Ishwar Kumar Mishra,[†] Jiming Bao,[§] Richard C. Willson,[‡] and Zhifeng Ren*[,†]

[†]Department of Physics and TcSUH, University of Houston, Houston, Texas 77204, United States

[‡]Department of Chemical and Biomolecular Engineering, University of Houston, Houston, Texas 77204, United States

[§]Department of Electrical and Computer Engineering, Materials Science and Engineering, University of Houston, Houston, Texas 77204, United States

Supporting Information

ABSTRACT: Colloidal behavior is fundamental for many applications. Methods for evaluating the stability of chemically homogeneous nanoparticles have been developed well. However, little attention has been paid to that of amphiphilic Janus nanomaterials that have recently emerged. In polar solvents, the significant influence of hydrophobic interaction complicated the evaluation of stability because of the lack of generally accepted theoretical energy potential for the interaction. To the best of our knowledge, this study is the first to investigate the colloidal stability of graphene-based amphiphilic Janus nanosheets at different salt concentrations and temperatures by developing a theoretical model with an understanding of the chemical and physical properties of the fluid. The model predictions were in good agreement with experimental stability evaluations. This study could also serve as a foundation for understanding the behavior of other amphiphilic Janus nanomaterials, achieving complex structures, and stabilizing the amphiphilic Janus nanomaterials for applications in unfriendly environments, e.g., at high salinities or temperatures.

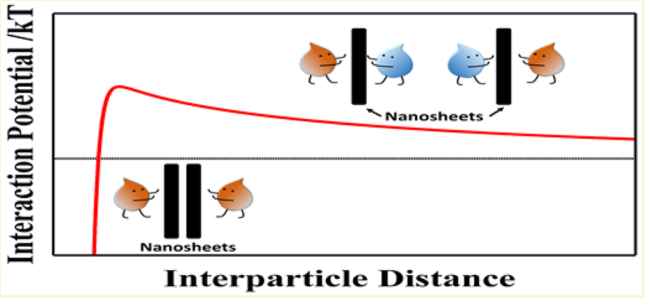

1. INTRODUCTION

The colloidal stability of chemically homogeneous nanoparticles,[1−6] including low-dimensional carbon nanotubes[7] and graphene oxide (GO),[8] has been extensively investigated for various applications, in many of which colloidal stability is a vital characteristic. Classical DLVO theory is a well-developed method for understanding the colloidal behavior of surface-charged homogeneous nanoparticles in polar solvents. This theory considers the balance between van der Waals (VDW) attractive forces and electrostatic repulsive forces.[9] When necessary, nanoparticle stability can be improved by adding stabilizers to provide steric stabilization,[10,11] generate depletion stabilization,[12,13] or enhance the electrostatic repulsion force.[14]

Amphiphilic Janus nanomaterials are colloids that have both hydrophilic and hydrophobic faces. They can exist at immiscible fluid interfaces for relatively long periods of time.[15] When amphiphilic Janus nanomaterials are dispersed in a polar solvent, hydrophobic force plays a significant role in determining the colloidal properties of these particles. However, there is no generally accepted theoretical energy potential for these hydrophobic interactions,[16] which complicates stability evaluations. Recently, a graphene-based amphiphilic Janus nanosheet fluid was discovered for oil recovery. This nanofluid showed record-high performance at very low concentrations because of the decrease in interfacial tension and formation of climbing and interfacial films at different hydrodynamic powers.[17] Before any material can be used for practical applications, however, such as implementation in seawater or an underground environment, it is crucial to understand the stability properties of the nanofluid. However, the stability of this material has not been theoretically or systematically investigated.

Graphene-based amphiphilic Janus nanosheets were synthesized by hydrophobizing one side of GO with alkylamine. Functionalization restored the graphitic sp2 network, which altered the surface electronic structure of GO.[18] This alteration could produce physical properties different from those of GO. To calculate interaction energy potentials between these colloids, the surface conjugation ratio (defined as the ratio of alkylamine-functionalized sites to the total available functional sites on the GO surface) and physical properties of the material must be determined. However, to the best of our knowledge, no studies have investigated this topic. The aim of this study was to develop a method for characterizing the colloidal

Received: December 4, 2016
Revised: March 7, 2017
Published: April 5, 2017

DOI: 10.1021/acs.chemmater.6b05148
Chem. Mater. 2017, 29, 3454−3460

behavior of amphiphilic Janus nanomaterials and the factors that affect it. This work could also provide a foundation for evaluating the stability of other amphiphilic Janus nanomaterials, controlling self-assembly to create more complex structures, and stabilizing nanosheets for applications in extreme environments, e.g., at high salinities or temperatures.

2. MATERIALS AND METHODS

2.1. Modeling Methods. To maximize the transport properties of graphene-based amphiphilic Janus nanosheets in rock pores, the lateral dimension was optimized to 100−300 nm. Following alkylamine conjugation, the nanosheet thickness was evaluated using atomic force microscopy (AFM) (Figure S1). The thickness was approximately 3.7 nm, which is similar to the previously reported value.[19] The nanosheet aspect ratio (the ratio of the lateral length to the thickness) ranged from 25 to 85, with all values being <100. Therefore, it is reasonable to use a two-sphere model to characterize interactions between nanosheets. We here considered VDW attractive potential, electrostatic repulsive potential, and hydrophobic interactive potential when modeling the interaction potential of the amphiphilic Janus nanosheets. The balance among these interactions defines the behavior of the nanosheets in aqueous solution.

The VDW interaction energy between two spheres is shown in eq 1:[20]

$$\varnothing_{VDW} = -\frac{H}{6}\left\{\frac{2R_1R_2}{f_1(R_1, R_2, d)} + \frac{2R_1R_2}{f_2(R_1, R_2, d)} + \ln\left[\frac{f_1(R_1, R_2, d)}{f_2(R_1, R_2, d)}\right]\right\} \quad (1)$$

$$f_1(R_1, R_2, d) = d^2 + 2R_1d + 2R_2d$$

$$f_2(R_1, R_2, d) = d^2 + 2R_1d + 2R_2d + 4R_1R_2$$

where H is the Hamaker constant, d is the separation of the nanoparticle surface, and R_1 and R_2 are the radii of the nanoparticles. The challenge of quantifying the VDW potential is determining the Hamaker constant. Because of the lack of a Hamaker constant of the nanosheets, the geometrical mixing rule was not applicable. Therefore, we used an approach based on Lifshitz theory to obtain the Hamaker constant for media 1 and 2 interacting across medium 3. All media were assumed to have the same absorption frequencies. Because the zero-frequency contribution is usually small, the approximate expression of the Hamaker constant can be reduced, as shown in eq 2.[21]

$$H \approx \frac{3h\nu_e}{8\sqrt{2}} \frac{(n_1^2 - n_3^2)(n_2^2 - n_3^2)}{(n_1^2 + n_3^2)^{1/2}(n_2^2 + n_3^2)^{1/2}[(n_1^2 + n_3^2)^{1/2} + (n_2^2 + n_3^2)^{1/2}]} \quad (2)$$

where h is Planck's constant, ν_e is the primary electronic absorption frequency in the UV region, and n is the refractive index in the visible regime. ν_e is approximated as $\nu_e = \nu_1\sqrt{3/(n_i^2 + 2)}$,[8] where ν_1 is the absorption frequency of a Bohr atom (3.3×10^{15} s^{-1}) and n_i the refractive index of the nanosheets. The nanofluid is composed of graphene-based amphiphilic Janus nanosheets dispersed in water. If a refractive index of 1.3325 is used for water,[22] the Hamaker constant can be estimated by determining the refractive index of graphene-based amphiphilic Janus nanosheets.

The ζ potential of amphiphilic Janus nanosheets in deionized (DI) water is approximately −22 mV, smaller than that of GO.[23] The reduced ζ potential is probably due to covalent bonding of an oxygen-containing group with alkylamine. For low surface potential at a constant surface charge density, the electrical double-layer interaction energy can be calculated as follows.[24]

$$\varnothing_{EL} = N_1\{N_2 f(d) - \ln[1 - \exp(-2\kappa d)]\} \quad (3)$$

$$N_1 = \pi\varepsilon_0\varepsilon_m R_1R_2(\psi_{0,1}^2 + \psi_{0,2}^2)/(R_1 + R_2)$$

$$N_2 = 2\psi_{0,1}\psi_{0,2}/(\psi_{0,1}^2 + \psi_{0,2}^2)$$

$$f(d) = \ln\{[1 + \exp(-\kappa d)]/[1 - \exp(-\kappa d)]\}$$

$$\kappa = [2e^2N_AI/(\varepsilon_0\varepsilon_m kT)]^{1/2}$$

where ε_0 is the vacuum permittivity, ε_m is the solvent permittivity, $\psi_{0,1}$ and $\psi_{0,2}$ are the surface potentials of nanoparticles, κ is the inverse Debye length, e is the elementary charge, N_A is Avogadro's number, I is the ionic strength, k is Boltzmann's constant, and T is the absolute temperature. We used the ζ potential as the surface potential. We calculated the temperature-dependent dielectric constant of water (ε_m) as $87.73 \times 10^{-0.002(T-273.15)}$.[25]

The hydrophobic surfaces of amphiphilic Janus nanosheets inherently attract each other and avoid water to minimize the free energy of the system. To quantify this interaction, we used an empirically derived potential in which the hydrophobic energy is related to interfacial tension and the amount of exposed hydrophobicity.[16,26] Because exposed hydrophobicity is closely correlated to the degree of surface conjugation, the interaction potential could be modified as follows:

$$\varnothing_{phobic} = -2A\gamma f_{pho/(pho+phi)}\exp(-d/D_o) \quad (4)$$

where A is the surface area of the hydrophobic side of the nanoparticle, γ is the interfacial tension of an alkylamine hydrocarbon molecule in water (40 mN/m), D_o is the hydrophobic decay length (1 nm),[27] and $f_{pho/(pho+phi)}$ is the surface conjugation ratio. The value of the surface conjugation ratio can be extracted from X-ray photoelectron spectroscopy (XPS) measurements.

2.2. Experimental Methods. The graphene-based amphiphilic Janus nanosheets were synthesized as described previously.[17] Briefly, graphite was first exfoliated and oxidized. Then, single-surface functionalization of the oxidized graphene with alkylamine was performed via a wax microsphere covering method. The nanofluid was prepared in deionized water followed by sonication. The refractive index of the amphiphilic Janus nanosheets was measured with reflection spectroscopy using the angle interrogation method, in which the light reflectivity is monitored as a function of the incident angle. A He−Ne laser (λ = 633 nm) was used as a light source, and only p-polarized light was used for the reflection measurement. The sample was prepared using drop casting, in which a few drops of nanofluid were placed on a glass slide and dried on a hot plate. We used atomic force microscopy (AFM) (Veeco Dimension 3000) to characterize the morphology of graphene-based amphiphilic Janus nanosheets. AFM was performed in tapping mode with a resolution of 512 × 512. Silicon AFM probes (HQ:NSC15/AL BS, Mikromasch) with tip radii of ∼8 nm were used to perform the measurement. The resonant frequency of the measurements was ∼325 kHz, and the force constant was ∼40 N m^{-1}. The ζ potential was measured using a Zetasizer Nano Z. The distance between particles was visualized using a Malvern Nanosight NS300 instrument. The chemical composition of amphiphilic Janus nanosheets was recorded using XPS (Physical Electronics model 5700). A Cary 5000 UV−vis−NIR spectrophotometer was employed to obtain UV−vis spectra.

3. RESULTS AND DISCUSSION

Six reflectivity measurements of the glass substrate were first collected in two different spots, as shown in Figure 1a. All of the graphs overlap each other, demonstrating that the measurement is repeatable. As depicted in Figure 1b, one of the six data sets was selected for simulation to find the Brewster's angle of the glass substrate, which was confirmed as

DOI: 10.1021/acs.chemmater.6b05148
Chem. Mater. 2017, 29, 3454−3460

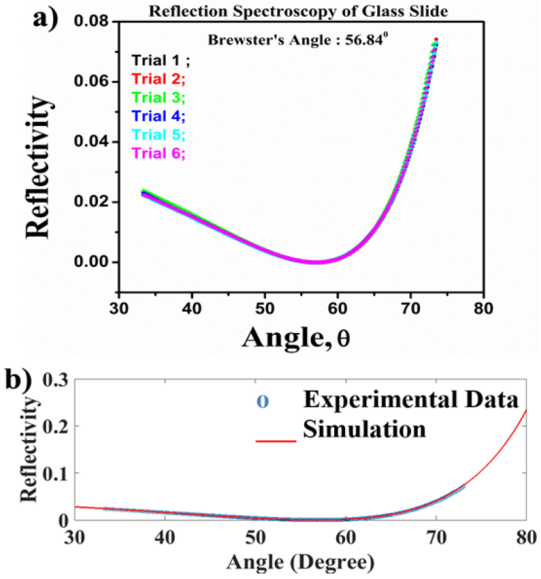

Figure 1. Refractive index measurements of the glass substrate. (a) Six measurements of the reflectivity of the glass substrate in two different spots. (b) Simulation result for calculating the refractive index of the glass substrate.

56.84°. The result is consistent with the refractive index of glass (1.53). Then, the refractive index of the amphiphilic Janus nanosheets was determined, and the experimental data were fitted using Fresnel's equation for a three-layer structure (Figure 2). The first layer was air; the second, nanosheets; and the third, the glass substrate. Reflectivity R for p-polarized light is given as follows.[28]

$$R = |r_{123}^{P}|^2 = \left| \frac{r_{12}^{P} + r_{23}^{P} \exp(2i\beta)}{1 + r_{12}^{P} r_{23}^{P} \exp(2i\beta)} \right|^2 \quad (5)$$

where

$$\beta = \frac{2\pi}{\lambda} n_2 \cos\theta_2 d$$

and

$$r_{ij}^{P} = \frac{n_j \cos\theta_i - n_i \cos\theta_j}{n_j \cos\theta_i + n_i \cos\theta_j}$$

where i and j equal 1, 2, or 3. The real part of the refractive index of the amphiphilic Janus nanosheets on the glass substrate was 1.58. Compared with the refractive indices of graphene and its related materials reported in the literature,[29−34] as shown in Table S1, the value falls into the reasonable range, and the difference was produced by the increased thickness of the nanosheet and single-side-functionalized oxidized graphene altering the conductivity, which affected the dielectric property and, thus, modified the refractive index.

On the basis of the use of a Shirley background, Gaussian convolution of the nanosheet C 1s XPS results yielded five fitted peaks (Figure 3) that were assigned as -C-C- (284.8 eV), -C-N- (285.4 eV), -C-OH (286.6 eV), -C-O-C- (287.1 eV), and -O-C═O (288.8 eV). Compared with GO, the additional -C-N- peak was introduced because of alkylamine conjugation, which corresponds to hydrophobic sites as the hydrocarbon chains.[35,36] In addition, the N peak around 400 eV was also

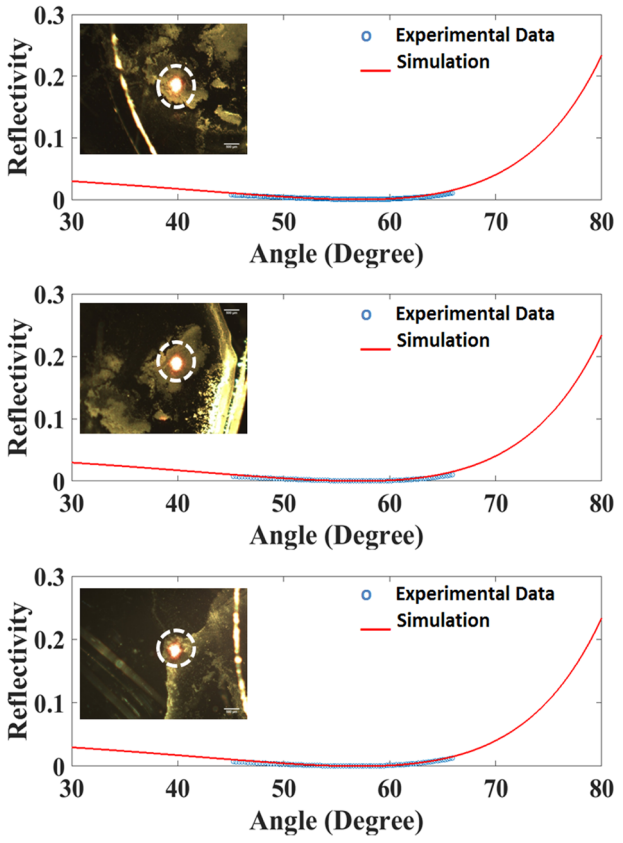

Figure 2. Refractive index measurements of graphene-based amphiphilic Janus nanosheets. Blue circles are experimental data, and solid red lines are simulated data. Insets show an optical image of the sample on glass substrates and the laser spot.

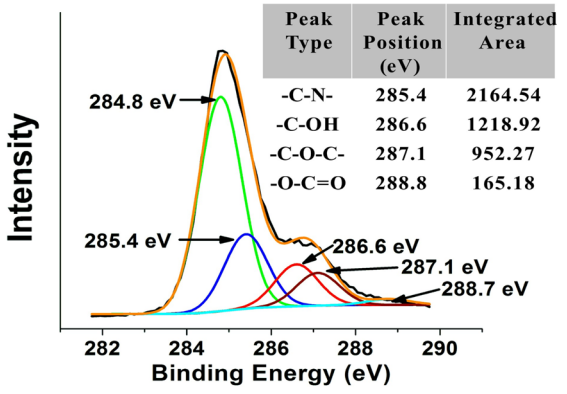

Figure 3. XPS measurement of graphene-based amphiphilic Janus nanosheets. The inset table shows the integrated areas of each fitted curve.

detected in XPS spectra, which further demonstrated the successful conjugation of alkylamine as depicted in Figure S2. Therefore, the surface conjugation ratio was quantified using the ratio of the -C-N- peak integrated area (2164.54) to the total integrated area of surface functional groups (4500.91). The surface conjugation ratio of the graphene-based amphiphilic Janus nanosheets was approximately 0.48.

The coordinates of amphiphilic Janus nanosheets were captured and visualized using a Nanosight NS300 at a nanosheet concentration of 0.005 wt %. This is the concentration used for oil recovery in our previous reports.[17]

DOI: 10.1021/acs.chemmater.6b05148
Chem. Mater. 2017, 29, 3454−3460

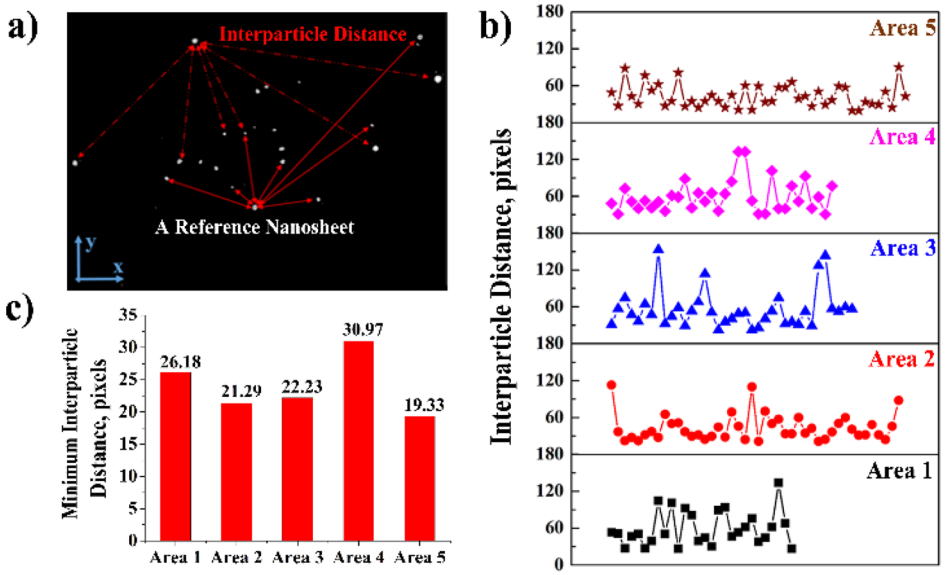

Figure 4. Interparticle distance. (a) The nanosheets were imaged using a Nanosight NS300 instrument. (b) Shortest interparticle distances of every reference nanosheet in five areas. (c) Minimal interparticle distances in five areas (1 pixel ≈ 160 nm).

The interparticle distance was calculated using light scattering (Figure 4a). One nanosheet was designated as the reference point. The interparticle distance between the reference and all other nanosheets in the same frame was calculated. Then, a different nanosheet was selected as a reference, and the calculation was repeated for every visible nanosheet. The shortest distance observed for each reference nanosheet and the minimal interparticle distance in five different areas are shown in panels b and c of Figure 4, respectively. The distance unit used was a pixel, and one pixel represents approximately 160 nm here. The averaged hydrodynamic diameter of the nanosheets was reported previously to be 120 nm.[17] After subtraction of the size of the nanosheet, the interparticle distance was at the micrometer level.

Once the refractive index and surface conjugation ratio were determined, we quantified the total interaction potential. Negative interaction potentials predict an unstable fluid system. For amphiphilic Janus nanomaterials, hydrophobic interactions cause a loss of stability in a polar solvent. Therefore, we first investigated the influence of hydrophobic interactions. When hydrophobic force is not included in the calculation, the nanofluid is theoretically stable at 0.01 mol of NaCl/L (Figure 5a). However, stability is lost once hydrophobic force is added to the calculation (Figure 5b). Experiments showed that amphiphilic Janus nanosheets aggregate and precipitate in 0.01 mol of NaCl/L because of ion screening effects (Figure 5d). Therefore, classical DLVO theory, which includes only VDW and electrostatic interaction, failed to evaluate the stability of amphiphilic Janus nanosheets. In practice, atmospheric carbon dioxide dissolves in DI water, leading to an ionic strength equivalent to 10^{-6} mol of NaCl/L at equilibrium.[37] In theory, the ratio of interaction potential to thermal energy at that ionic strength would be >30 at an interparticle distance of 1000 nm (Figure 5b), i.e., the experimentally determined distance of the nanosheets mentioned above. On the basis of this ratio, graphene-based amphiphilic Janus nanosheets should stably disperse in DI water. This theory was consistent with our experimental observations (Figure 5d). In addition, the hydrophobic force increased the minimal requirement for stable interparticle distances, which is highlighted by the

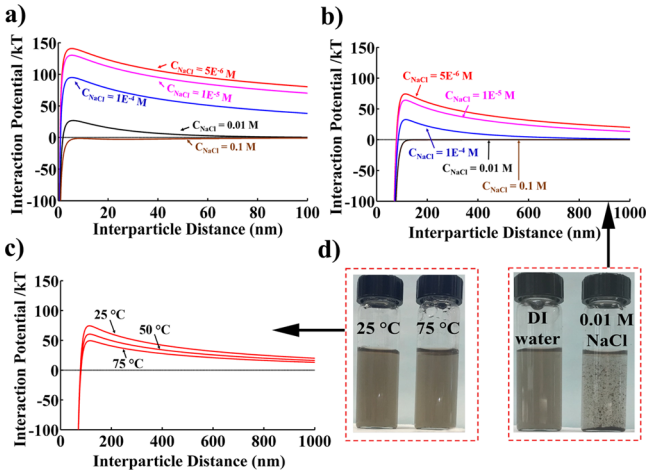

Figure 5. Stability evaluation. (a) Interaction potential at varying interparticle distances for different salt concentrations without accounting for hydrophobic force. (b) Interaction potential at varying interparticle distances for different salt concentrations when accounting for hydrophobic force. (c) Interaction potential at varying interparticle distances for different temperatures. (d) Stability testing of the nanofluid at different temperatures (left red dashed box) and salt concentrations (right red dashed box) for several hours.

shifting zero-potential points for these curves at very low salt concentrations, i.e., 5×10^{-6}, 1×10^{-5}, and 1×10^{-4} mol/L. Furthermore, when the temperature was increased from 25 to 75 °C, the interaction potential curve did not change appreciably and the nanofluid maintained its stability (Figure 5c). When the nanofluid was tested experimentally, there was no observable aggregation in the nanofluid after several hours at 75 °C (Figure 5d).

A UV−vis spectrophotometer was further used to characterize the colloidal stability as the decrease in intensity may reflect a change in particle concentration, which may be caused by agglomeration. After the samples had settled for 5 h, the spectra of amphiphilic Janus nanosheet dispersions with the same concentrations in DI water as well as in three other NaCl solutions (10^{-5}, 10^{-4}, and 10^{-2} M) were recorded as shown in

DOI: 10.1021/acs.chemmater.6b05148
Chem. Mater. 2017, 29, 3454−3460

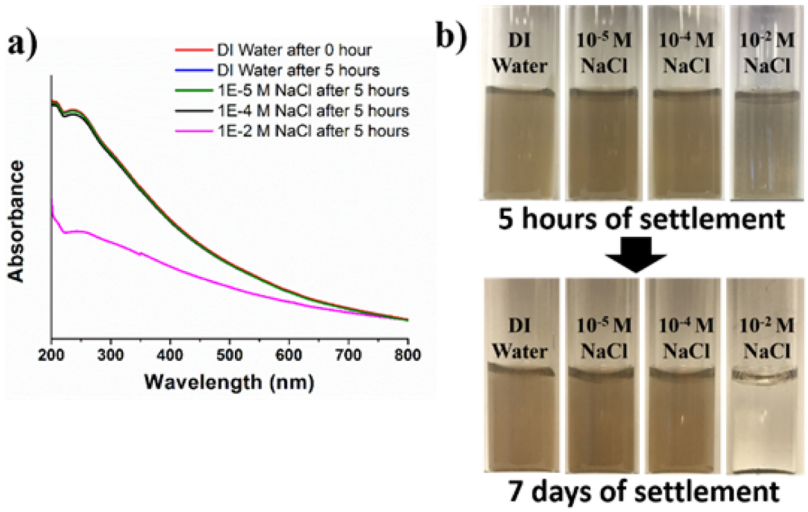

Figure 6. (a) UV−vis spectra of graphene-based amphiphilic Janus nanosheets in different solutions after a certain period of settling. (b) Visual stability evaluation after nanosheets had settled for 5 h and 7 days.

Figure 6a. Amphiphilic nanosheets in 10^{-4} and 10^{-5} M NaCl solutions after settling for 5 h and in DI water after settling for 0 and 5 h all displayed quite similar spectra with little difference. On the other hand, the spectrum of amphiphilic nanosheets in a 10^{-2} M NaCl solution gave a significantly lower intensity. After settling overnight, the nanosheets dispersed in a 10^{-2} M NaCl solution completely precipitated. However, amphiphilic nanosheets in water and NaCl solutions at concentrations of 10^{-5} and 10^{-4} M displayed negligible precipitation even after settling for 7 days.

At certain interparticle distances, the hydrophobic attraction would become the dominant interaction compared with electrical double-layer repulsive interaction as calculated and shown in Figure S3. The domination distance is ~80 nm. For a Debye length at the same level of that distance (approximately 95 nm for a solution with a 10^{-5} M NaCl concentration and 134 nm in DI water), the interaction potential of an electrical double layer for nonspherical particles beyond the hydrophobic domination distance can be expressed as the potential of its effective spherical particles times the anisotropic function.[38,39] The anisotropic function depends on the value of inverse Debye length κ, multiplied by half the length of the lateral size of the nanosheets (l_{half}) and also on the angle between them. As mentioned above, the aspect ratio of the nanosheets with a 3.7 nm thickness is between 25 and 85 (<100). Therefore, the range of κl_{half} is from 0.34 to 1.7 (<2), which shows the anisotropic effect is not significant under the constant surface charge density assumption.[39] In addition, the particle distance for DI water was measured at the micrometer level, and the interaction itself was weak. Therefore, using a two-sphere model here with an aspect ratio of <100 is reasonable, and the modeling results match well with those of the experimental testing.

As mentioned above, 0.01 mol/L (0.05844 wt %) NaCl destabilizes the nanofluid. To disperse amphiphilic Janus nanosheets on the surface with seawater or in high-saline water for oil recovery in the future, we will need to find appropriate stabilizers that permit this dispersion while maintaining the unique interfacial behavior of the nanosheets when reaching underground.

4. CONCLUSIONS

In summary, we devised a method of theoretically investigating the colloidal stability of graphene-based amphiphilic Janus nanosheets and the factors affecting it.

The Hamaker constant of graphene-based amphiphilic Janus nanosheets has been determined by obtaining the refractive index of the nanosheets with the help of reflection measurement, which was the key to quantifying the van der Waals interaction potential.

A modified expression for calculating the hydrophobic interaction was proposed by using the parameter of the surface conjugation ratio of the nanosheets, which can be extracted from XPS data.

The influence of hydrophobic interaction on stability evaluation was also investigated and verified by experiments, which demonstrated that classical DLVO theory failed to study the colloidal behavior for amphiphilic Janus nanomaterials.

The factors, including ionic strength and temperature, affecting the fluid stability have been discussed. The results were in good agreement with results of both UV−vis and visual stability testing under such conditions, validating the method presented here for colloidal stability evaluation of the amphiphilic Janus nanosheets.

■ ASSOCIATED CONTENT

Supporting Information

The Supporting Information is available free of charge on the ACS Publications website at DOI: 10.1021/acs.chemmater.6b05148.

AFM image of graphene-based amphiphilic Janus nanosheets, refractive indices of graphene-related materials reported in the literature, XPS spectra of unfitted C1S and N1S of graphene-based amphiphilic Janus nanosheets, and curves of hydrophobic and electrical double-layer interaction over the interpartcle distance (PDF)

■ AUTHOR INFORMATION

Corresponding Author

*E-mail: zren@uh.edu.

ORCID

Jiming Bao: 0000-0002-6819-0117

DOI: 10.1021/acs.chemmater.6b05148
Chem. Mater. 2017, 29, 3454−3460

Zhifeng Ren: 0000-0001-8233-3332

Notes

The authors declare no competing financial interest.

■ ACKNOWLEDGMENTS

The work performed at the University of Houston is supported by the U.S. Department of Energy under Contract DE-SC0010831. J.M.B. acknowledges support from the National Science Foundation (Career Award ECCS-1240510) and the Robert A Welch Foundation (E-1728).

■ REFERENCES

(1) Lee, H. J.; Choi, H. W.; Kim, K. J.; Lee, S. C. Modification of Hydroxyapatite Nanosurfaces for Enhanced Colloidal Stability and Improved Interfacial Adhesion in Nanocomposites. *Chem. Mater.* **2006**, *18*, 5111−5118.

(2) Mak, W. C.; Cheung, K. Y.; Trau, D. Influence of Different Polyelectrolytes on Layer-by-Layer Microcapsule Properties: Encapsulation Efficiency and Colloidal and Temperature Stability. *Chem. Mater.* **2008**, *20*, 5475−5484.

(3) Giljohann, D. A.; Seferos, D. S.; Prigodich, A. E.; Patel, P. C.; Mirkin, C. A. Gene Regulation With Polyvalent siRNA-Nanoparticle Conjugates. *J. Am. Chem. Soc.* **2009**, *131*, 2072−2073.

(4) Mulvihill, M. J.; Habas, S. E.; Jen-La Plante, I.; Wan, J.; Mokari, T. Influence of Size, Shape, and Surface Coating on the Stability of Aqueous Suspensions of CdSe Nanoparticles. *Chem. Mater.* **2010**, *22*, 5251−5257.

(5) Lin, Y. S.; Abadeer, N.; Haynes, C. L. Stability of Small Mesoporous Silica Nanoparticles in Biological Media. *Chem. Commun.* **2011**, *47*, 532−534.

(6) Terlan, B.; Levin, A. A.; Börrnert, F.; Simon, F.; Oschatz, M.; Schmidt, M.; Cardoso-Gil, R.; Lorenz, T.; Baburin, I. A.; Joswig, J. O.; Eychmüller, A. Effect of Surface Properties on the Microstructure, Thermal, and Colloidal Stability of VB_2 Nanoparticles. *Chem. Mater.* **2015**, *27*, 5106−5115.

(7) Vaisman, L.; Wagner, H. D.; Marom, G. The Role of Surfactants in Dispersion of Carbon Nanotubes. *Adv. Colloid Interface Sci.* **2006**, *128−130*, 37−46.

(8) Gudarzi, M. M. Colloidal Stability of Graphene Oxide: Aggregation in Two Dimensions. *Langmuir* **2016**, *32*, 5058−5068.

(9) Moore, T. L.; Rodriguez-Lorenzo, L.; Hirsch, V.; Balog, S.; Urban, D.; Jud, C.; Rothen-Rutishauser, B.; Lattuada, M.; Petri-Fink, A. Nanoparticle Colloidal Stability in Cell Culture Media and Impact on Cellular Interactions. *Chem. Soc. Rev.* **2015**, *44*, 6287−6305.

(10) Shah, P. S.; Holmes, J. D.; Doty, R. C.; Johnston, K. P.; Korgel, B. A. Steric Stabilization of Nanocrystals in Supercritical CO_2 Using Fluorinated Ligands. *J. Am. Chem. Soc.* **2000**, *122*, 4245−4246.

(11) Belfield, K. D.; Zhang, L. Norbornene-Functionalized Diblock Copolymers via Ring-Opening Metathesis Polymerization for Magnetic Nanoparticle Stabilization. *Chem. Mater.* **2006**, *18*, 5929−5936.

(12) Zhang, X.; Servos, M. R.; Liu, J. Ultrahigh Nanoparticle Stability against Salt, PH, and Solvent with Retained Surface Accessibility via Depletion Stabilization. *J. Am. Chem. Soc.* **2012**, *134*, 9910−9913.

(13) Semenov, A. N.; Shvets, A. A. Theory of Colloid Depletion Stabilization by Unattached and Adsorbed Polymers. *Soft Matter* **2015**, *11*, 8863−8878.

(14) Mudunkotuwa, I. A.; Grassian, V. H. Citric Acid Adsorption on TiO_2 Nanoparticles in Aqueous Suspensions at Acidic and Circumneutral pH: Surface Coverage, Surface Speciation, and Its Impact on Nanoparticle-Nanoparticle Interactions. *J. Am. Chem. Soc.* **2010**, *132*, 14986−14994.

(15) Kumar, A.; Park, B. J.; Tu, F.; Lee, D. Amphiphilic Janus Particles at Fluid Interfaces. *Soft Matter* **2013**, *9*, 6604−6617.

(16) Donaldson, S. H.; Lee, C. T.; Chmelka, B. F.; Israelachvili, J. N. General Hydrophobic Interaction Potential for Surface/Lipid Bilayers from Direct Force Measurements Between Light-Modulated Bilayers. *Proc. Natl. Acad. Sci. U. S. A.* **2011**, *108*, 15699−15704.

(17) Luo, D.; Wang, F.; Zhu, J.; Cao, F.; Liu, Y.; Li, X.; Willson, R. C.; Yang, Z. Z.; Chu, C. W.; Ren, Z. Nanofluid of Graphene-based Amphiphilic Janus Nanosheets for Tertiary or Enhanced Oil Recovery: High Performance at Low Concentration. *Proc. Natl. Acad. Sci. U. S. A.* **2016**, *113*, 7711−7716.

(18) Li, W.; Tang, X. Z.; Zhang, H. B.; Jiang, Z. G.; Yu, Z. Z.; Du, X. S.; Mai, Y. W. Simultaneous Surface Functionalization and Reduction of Graphene Oxide With Octadecylamine for Electrically Conductive Polystyrene Composites. *Carbon* **2011**, *49*, 4724−4730.

(19) Wu, H.; Yi, W.; Chen, Z.; Wang, H.; Du, W. Janus Graphene Oxide Nanosheets Prepared via Pickering Emulsion Template. *Carbon* **2015**, *93*, 473−483.

(20) Hiemenz, P. C.; Rajagopalan, R. *Principles of Colloid and Surface Chemistry*, 3rd ed. (revised and expanded); CRC Press: New York, 1997; Chapter 10.

(21) Israelachvili, J. N. *Intermolecular and surface forces*, 3rd ed. (revised); Academic Press: Waltham, MA, 2011; Chapter 6.

(22) Scott, T. A., Jr. Refractive Index of Ethanol-Water Mixtures and Density and Refractive Index of Ethanol-Water-Ethyl Ether Mixtures. *J. Phys. Chem.* **1946**, *50*, 406−412.

(23) Konkena, B.; Vasudevan, S. Understanding Aqueous Dispersibility of Graphene Oxide and Reduced Graphene Oxide Through pK_a Measurements. *J. Phys. Chem. Lett.* **2012**, *3*, 867−872.

(24) Hogg, R.; Healy, T. W.; Fuerstenau, D. W. Mutual Coagulation of Colloidal Dispersions. *Trans. Faraday Soc.* **1966**, *62*, 1638−1651.

(25) Maryott, A. A.; Malmberg, C. G. Dielectric Constant of Water from 0° to 100 °C. *J. Res. Natl. Inst. Stand. Technol.* **1956**, *56*, 1−8.

(26) Sanchez-Iglesias, A.; Grzelczak, M.; Altantzis, T.; Goris, B.; Perez-Juste, J.; Bals, S.; Van Tendeloo, G.; Donaldson, S. H., Jr.; Chmelka, B. F.; Israelachvili, J. N.; Liz-Marzan, L. M. Hydrophobic Interactions Modulate Self-Assembly of Nanoparticles. *ACS Nano* **2012**, *6*, 11059−11065.

(27) Meyer, E. E.; Rosenberg, K. J.; Israelachvili, J. Recent Progress in Understanding Hydrophobic Interactions. *Proc. Natl. Acad. Sci. U. S. A.* **2006**, *103*, 15739−15746.

(28) Raether, H. *Surface Plasmons on Smooth and Rough Surfaces and on Gratings*; Springer-Verlag: Berlin, 1988; Chapter 2.

(29) Xue, T.; Cui, X.; Chen, J.; Liu, C.; Wang, Q.; Wang, H.; Zheng, W. A Switch of the Oxidation State of Graphene Oxide on a Surface Plasmon Resonance Chip. *ACS Appl. Mater. Interfaces* **2013**, *5*, 2096−2103.

(30) Jung, I.; Vaupel, M.; Pelton, M.; Piner, R.; Dikin, D. A.; Stankovich, S.; An, J.; Ruoff, R. S. Characterization of Thermally Reduced Graphene Oxide by Imaging Ellipsometry. *J. Phys. Chem. C* **2008**, *112*, 8499−8506.

(31) Bruna, M.; Borini, S. Optical constants of graphene layers in the visible range. *Appl. Phys. Lett.* **2009**, *94*, 031901−031903.

(32) Stebunov, Y. V.; Aftenieva, O. A.; Arsenin, A. V.; Volkov, V. S. Highly Sensitive and Selective Sensor Chips with Graphene-Oxide Linking Layer. *ACS Appl. Mater. Interfaces* **2015**, *7*, 21727−21734.

(33) Jung, I. Optical and electrical characterization of graphene-based material. Ph.D. Thesis, Northwestern University, Evanston, IL, 2007.

(34) Cheon, S.; Kihm, K. D.; Kim, H. G.; Lim, G.; Park, J. S.; Lee, J. S. How to Reliably Determine the Complex Refractive Index (RI) of Graphene by Using Two Independent Measurement Constrains. *Sci. Rep.* **2014**, *4*, 6364.

(35) Tan, M. T.; Liu, X.; Li, W.; Li, H. X. Enhancing Sorption Capacities for Copper(II) and Lead(II) under Weakly Acidic Conditions by L-Tryptophan-Functionalized Graphene Oxide. *J. Chem. Eng. Data* **2015**, *60*, 1469−1475.

(36) Dreyer, D. R.; Park, S.; Bielawski, C. W.; Ruoff, R. S. The chemistry of graphene oxide. *Chem. Soc. Rev.* **2010**, *39*, 228−240.

(37) McLean, E. O. Soil pH and lime requirement. *Methods of soil analysis. Part 2. Chemical and microbiological properties*; American Society of Agronomy, Soil Science Society of America: Washington, DC, 1982; pp 199−224.

DOI: 10.1021/acs.chemmater.6b05148
Chem. Mater. 2017, 29, 3454−3460

(38) Agra, R.; Trizac, E.; Bocquet, L. The interplay between screening properties and colloid anisotropy: Towards a reliable pair potential for disc-like charged particles. *Eur. Phys. J. E: Soft Matter Biol. Phys.* **2004**, *15*, 345−357.
(39) Álvarez, C.; Téllez, G. Screening of charged spheroidal colloidal particles. *J. Chem. Phys.* **2010**, *133*, 144908.

DOI: 10.1021/acs.chemmater.6b05148
Chem. Mater. 2017, 29, 3454−3460